Fast Gelatinized Asymmetric Adhesive Hydrogel for Enhanced Wearable Sensor Performance

Jiawei Liu[a], Qiang Tian [b], Lei Ye[d], Luqing Zhang[a], Zhaoran Wang[a], Jin Li [c]*, Yabin Zhang[a]*

[a]*Shandong Provincial Key Laboratory of Fluorine Chemistry and Chemical Materials, School of Chemistry and Chemical Engineering, University of Jinan, Jinan 250022, China*

[b]*Department of Senile Neurology, The Affiliated Taian City Central Hospital of Qingdao University, Taian,29 Longtan Road, 271000, China*

[c]*Department of Ophthalmology, The Affiliated Taian City Central Hospital of Qingdao University, Taian, 29 Longtan Road, 271000, China*

[d]*NMPA Key Laboratory for Technology Research and Evaluation of Drug Products and Key Laboratory of Chemical Biology (Ministry of Education), Department of Pharmaceutics, School of Pharmaceutical Sciences, Cheeloo College of Medicine, Shandong University, Jinan 250012, China*

Corresponding authors

*(Yabin Zhang) E-mail: chm_zhangyb@ujn.edu.cn

*(Jin Li) E-mail: tyfylj@163.com

In this work, vinyl imidazole and methyl chloroacetate were initially combined to synthesize 1-vinyl-3-methoxycarbonyl-imidazole, which was subsequently reacted with KOH to yield 1-vinyl-3-carboxyimidazole. The ^{1}H-NMR spectrum of 1-vinyl-3-methoxycarbonyl-imidazole is shown in Fig. S1, with peaks at 7.7 ppm (d, ^{1}H, CH_2=CH-N), 7.2 ppm (s, ^{1}H, CH_2=CH-N), 5.9 ppm (s, ^{1}H, N-CH=CH), 5.5 ppm (s, ^{1}H, N-CH=CH), 5.2 ppm (d, ^{1}H, N-CH_2-C), and 3.8 ppm (t, ^{1}H, C-O-CH_3). The ^{1}H-NMR spectrum of the Imidazolyl zwitterion (IZ) 1-vinyl-3-carboxyimidazole is shown in Fig. S2, with peaks at 7.7 ppm (d, ^{1}H, CH_2=CH-N), 7.2 ppm (s, ^{1}H, CH_2=CH-N), 5.8 ppm (s, ^{1}H, N-CH=CH), 5.4 ppm (s, ^{1}H, N-CH=CH), and 4.8 ppm (d, ^{1}H, N-CH_2-C).

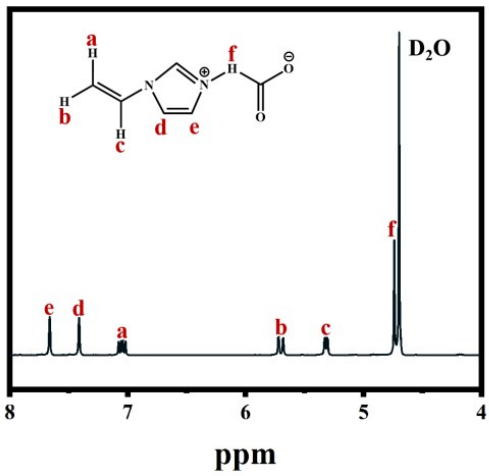

Fig. S1 ^{1}H-NMR spectrum of 1-vinyl-3-methoxycarbonyl-imidazole.

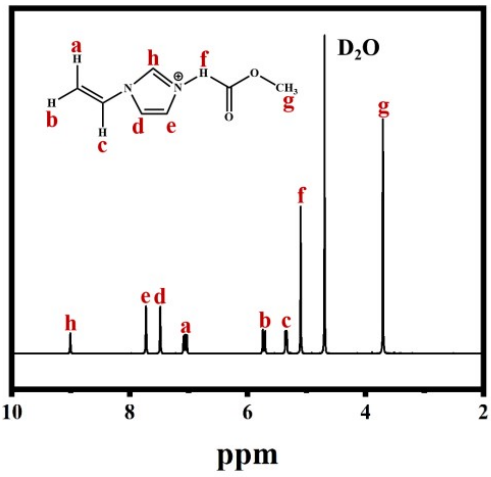

Fig. S2 ^{1}H-NMR spectrum of 1-vinyl-3-carboxyimidazole.

Fig. S3 Photos of the hydrogels being shaped into various shapes.

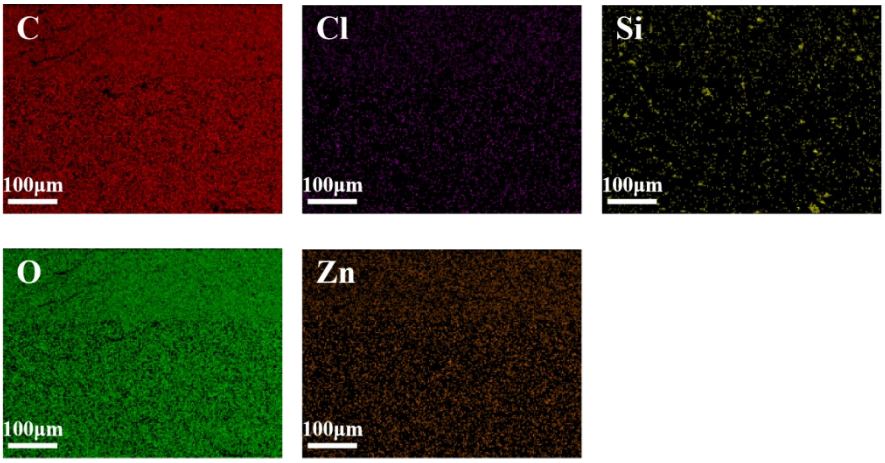

Fig. S4 EDS map of the hydrogel.

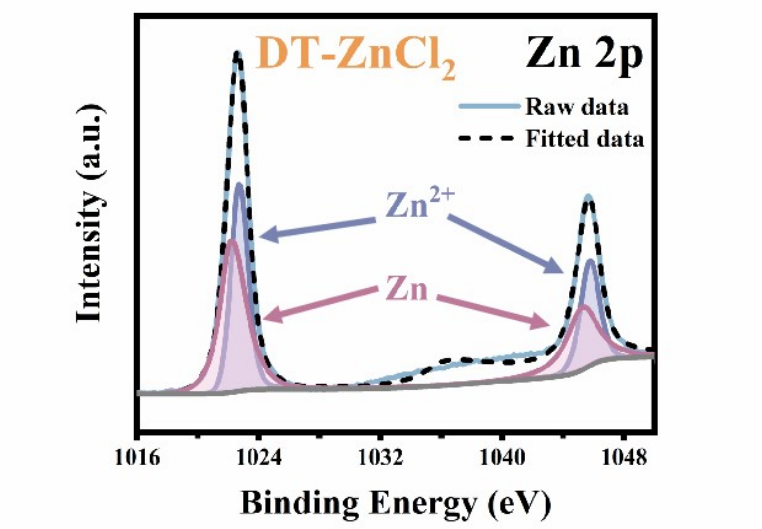

Fig. S5 High-resolution Zn 2p spectra for the DT-$ZnCl_2$ sample.

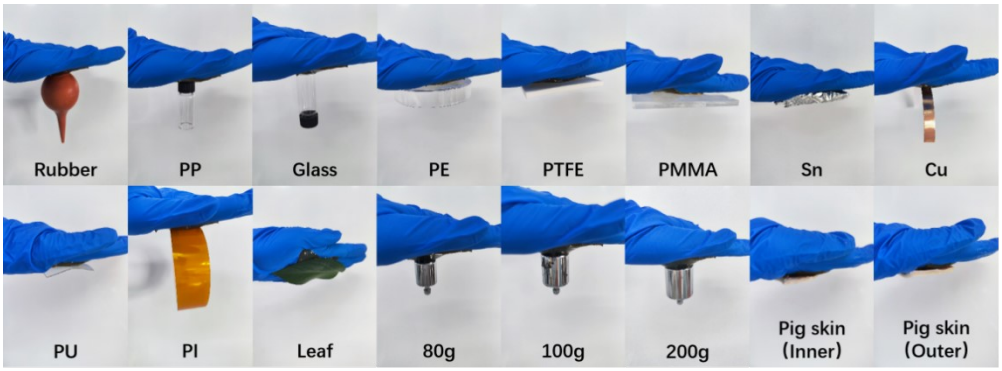

Fig. S6 Adhesion photos of DT_3 hydrogel adhering to various substrates (rubber, PP, glass, PE, PTFE, PMMA, tin, copper, PU, PI, leaves, and pig skin) and to different weights (80 g, 100 g, and 200 g).

Fig. S7 Photos of hydrogel adhering to human skin for 12 h after peeling off without residue or allergy.

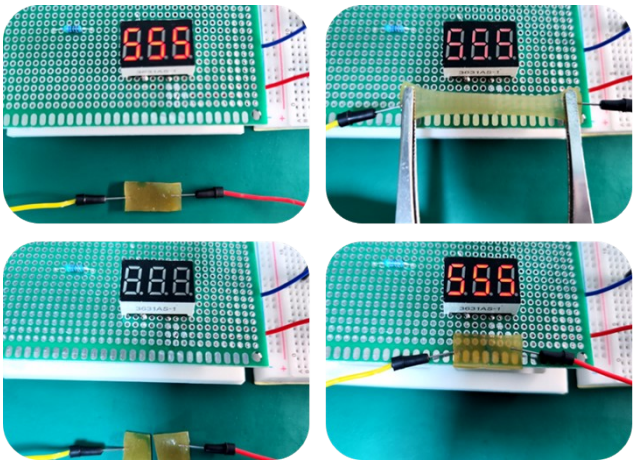

Fig. S8 Photos illustrate the connection of hydrogel to the circuit for displaying the numbers on the electronic meter.

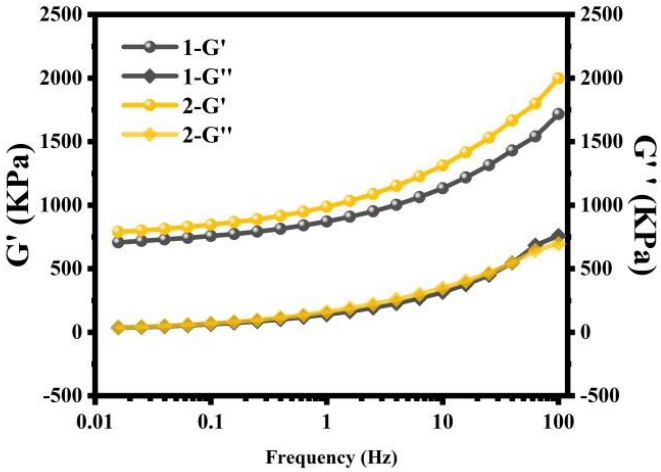

Fig. S9 Storage modulus and loss modulus of inner and outer hydrogels varying with frequency.

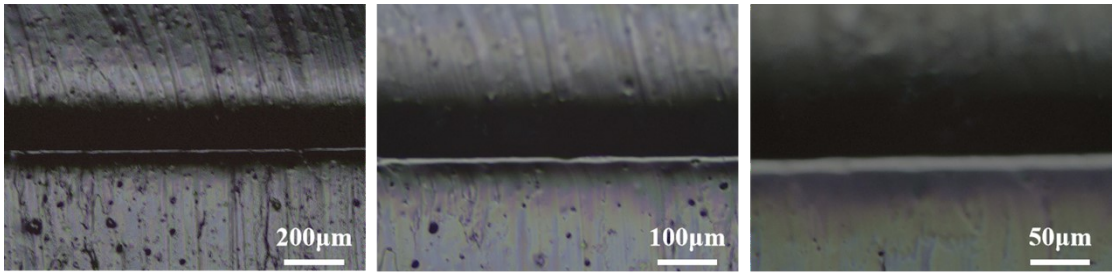

Fig. S10 Polarized light microscopy images of the boundary within the dual-layer hydrogel at different magnifications.

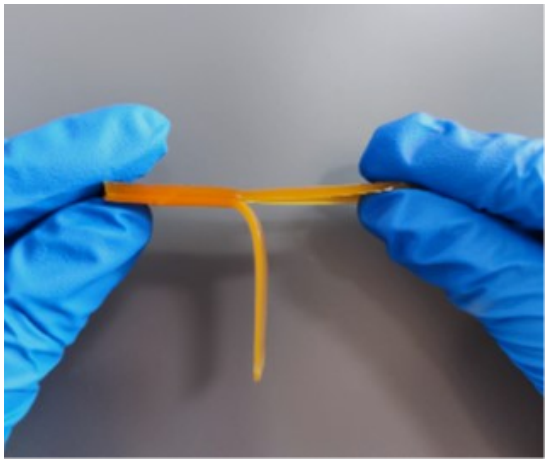

Fig. S11 Photographic image of the dual-layer hydrogel with half bound and half unbound for interfacial force test.

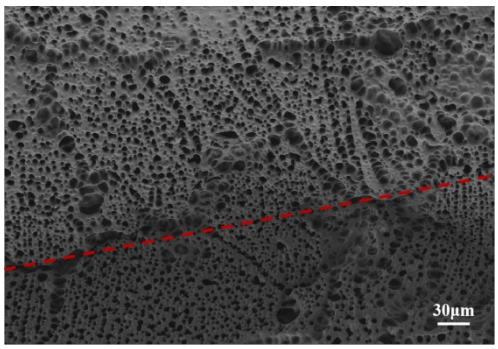

Fig. S12 SEM image of the dual-layer hydrogel after swelling and lyophilization.

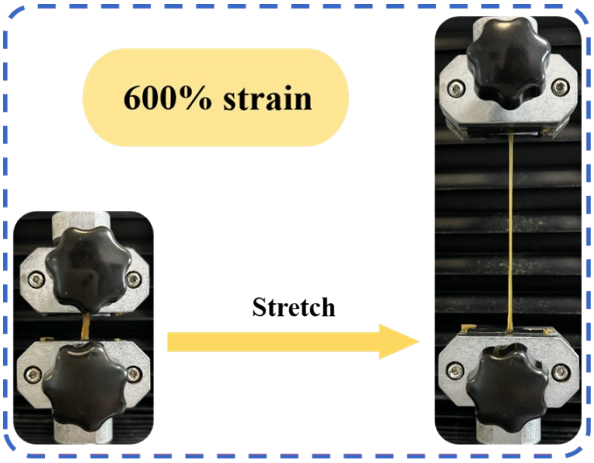

Fig. S13 Photographic images of the dual-layer hydrogel stretched to 600% strain.

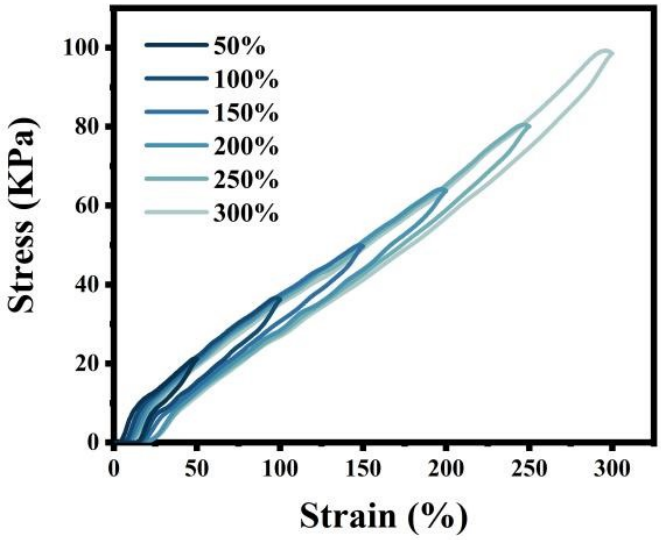

Fig. S14 Continuous loading and unloading stress-strain curves of dual-layer hydrogels under 50%-300% strain.

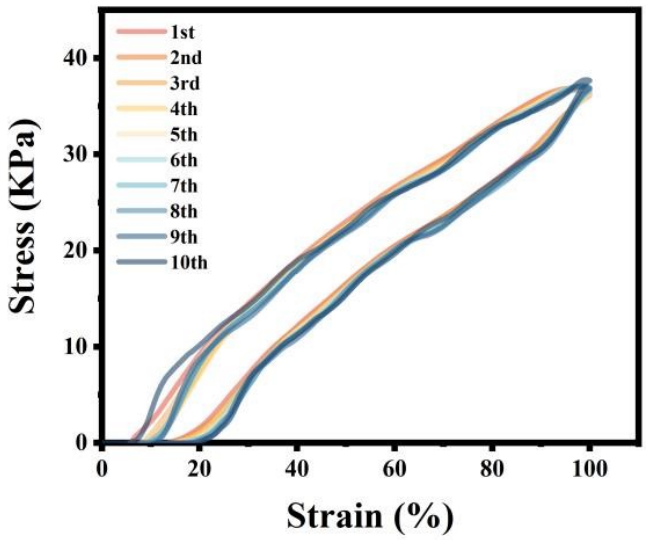

Fig. S15 Stress-strain curves of the dual-layer hydrogels under 10 cycles of stretching and releasing at 100% strain.

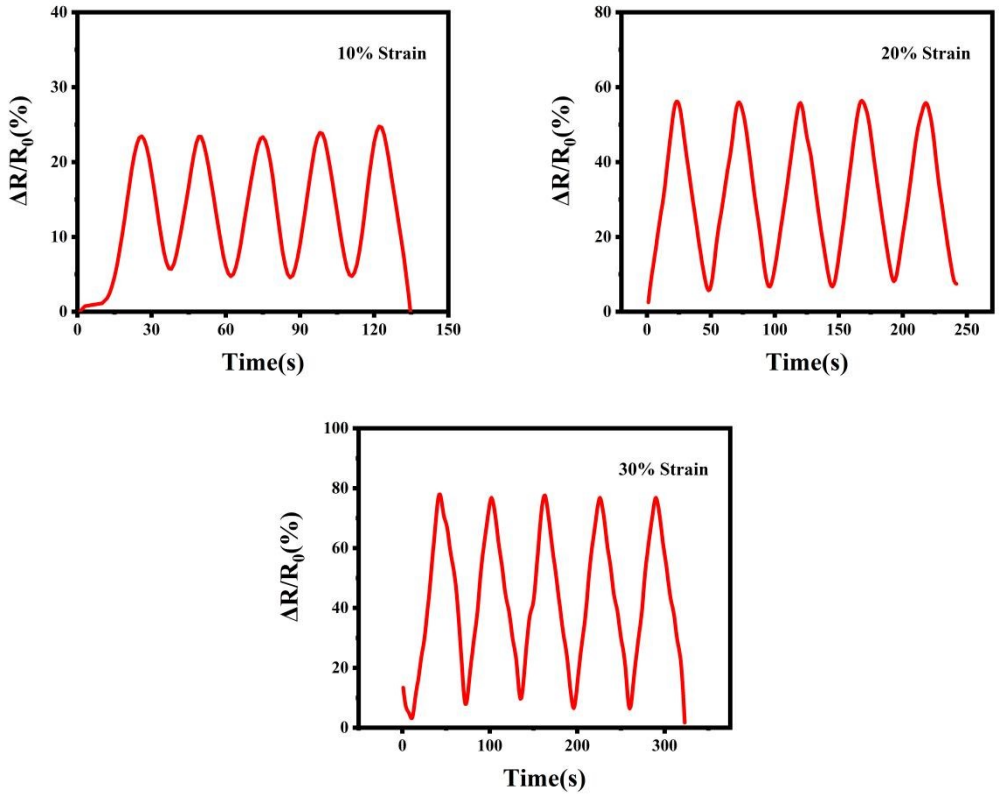

Fig. S16 Relative resistance changes under 10%, 20% and 30% strain in five cycles.

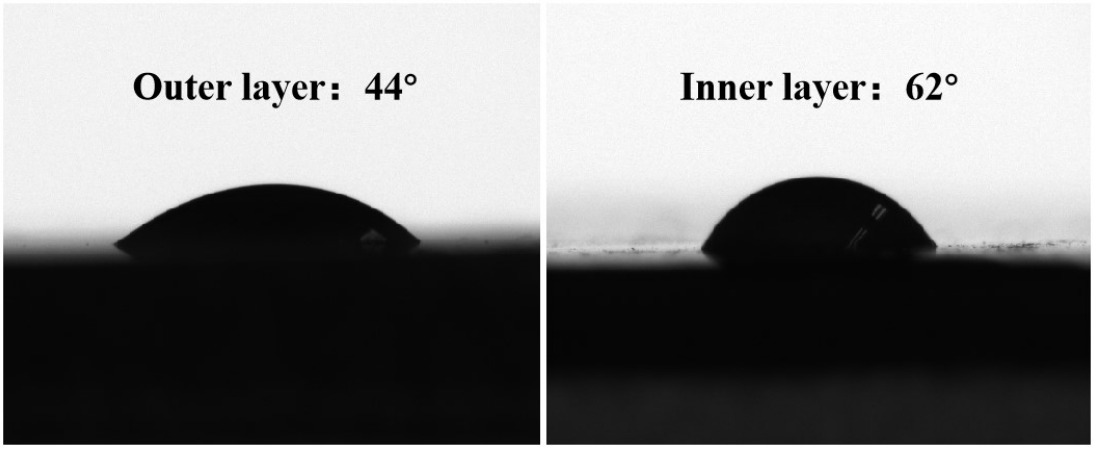

Fig. S17 Water contact angle of inner and outer layer of the hydrogels.

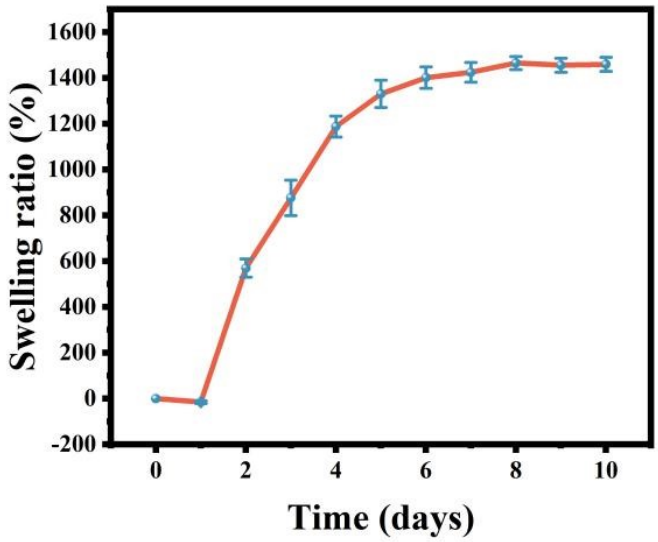

Fig. S18 Swelling ratio of inner hydrogel immersed in PBS buffer for 10 days.

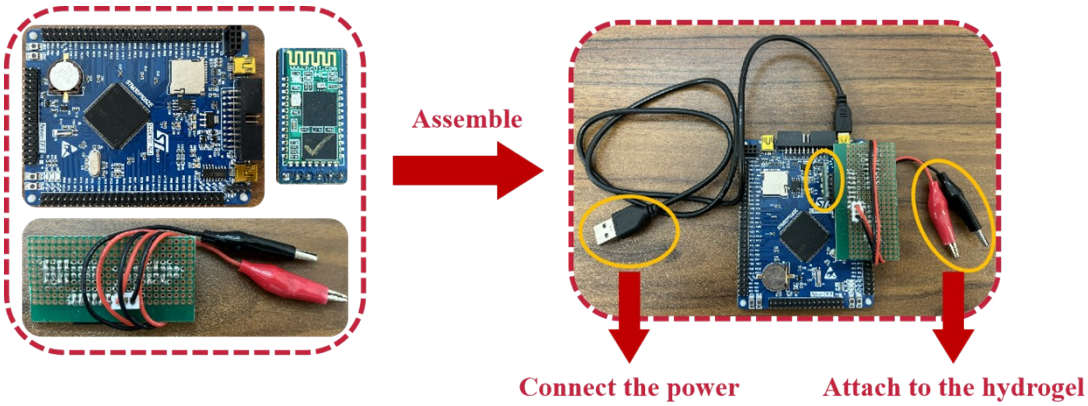

Fig. S19 Composition and use instructions of the Bluetooth wireless communication module.

Table 1. Nomenclature of the hydrogels with different $ZnCl_2$ mass fractions.

Codes	DE(g)	TA(g)	$ZnCl_2$(g)	AA(g)	IZ(g)	APS(mg)	MBA(mg)	H_2O(g)
PZA	0	0	0	4.5	0.9	50	20	10
DT-PZA	0.1	0.1	0	4.5	0.9	50	20	10
DT-4-PZA	0.1	0.1	5.46	4.5	0.9	50	20	10
DT-5-PZA	0.1	0.1	6.82	4.5	0.9	50	20	10
DT-6-PZA	0.1	0.1	8.18	4.5	0.9	50	20	10
DT-7.5-PZA	0.1	0.1	10.23	4.5	0.9	50	20	10

Table 2. Nomenclature of the hydrogels with different IZ mass fractions.

Codes	DE(g)	TA(g)	$ZnCl_2$(g)	AA(g)	IZ(g)	APS(mg)	MBA(mg)	H_2O(g)
IZ1	0.1	0.1	6.82	4.5	0.45	50	20	10
IZ2	0.1	0.1	6.82	4.5	0.9	50	20	10
IZ3	0.1	0.1	6.82	4.5	1.35	50	20	10
IZ4	0.1	0.1	6.82	4.5	1.8	50	20	10
IZ5	0.1	0.1	6.82	4.5	2.25	50	20	10

Table 3. Nomenclature of the hydrogels with different TA mass fractions.

Codes	DE(g)	TA(g)	$ZnCl_2$(g)	AA(g)	IZ(g)	APS(mg)	MBA(mg)	H_2O(g)
DT0.3	0.1	0.03	6.82	4.5	0.9	50	20	10
DT0.5	0.1	0.05	6.82	4.5	0.9	50	20	10
DT1	0.1	0.1	6.82	4.5	0.9	50	20	10
DT2	0.1	0.2	6.82	4.5	0.9	50	20	10
DT3	0.1	0.3	6.82	4.5	0.9	50	20	10

Table 4. Effect of components on rapid gelation.

Codes	DE(g)	TA(g)	$ZnCl_2$(g)	AA(g)	IZ(g)	APS(mg)	MBA(mg)	H_2O(g)
No gelation	0	0	0	4.5	0.9	50	20	10
	0.1	0.1	0	4.5	0.9	50	20	10
	0	0	6.82	4.5	0.9	50	20	10
Rapid gelation	0.1	0.03	6.82	4.5	0.9	50	20	10
	0.1	0.1	6.82	4.5	0.9	50	20	10
	0.1	0.3	6.82	4.5	0.9	50	20	10

Video S1-S8.

Video S1. Demonstration of the process of forming hydrogel.

Video S2. Anti-cutting test of the hydrogel.

Video S3. Puncture resistance test of the hydrogel.

Video S4. Flame resistance test of the hydrogel.

Video S5. Stretching the hydrogels causes the light bulb to change in brightness.

Video S6. Demonstration of asymmetric adhesion properties of dual-layer hydrogels.

Video S7. Stretching process of the dual-layer hydrogel.

Video S8. Demonstration of Bluetooth sensor.